Comparative Study of PAM and Field-Oriented Sensorless Control for High-Speed PMSMs

Batoul ZBIB, Ferhat CHABOUR, Georges BARAKAT
Laboratoire GREAH, Université Le Havre Normandie, Le Havre, 76600, France, batoulzbib@hotmail.com

ABSTRACT -Permanent Magnet Synchronous Motors (PMSMs) are used to drive high-speed compressors for air conditioning in electric vehicles due to their high power density and efficiency. Robust control of PMSMs typically requires accurate rotor position information, which, for this type of application, often depends on costly and complex sensors—making it impractical for cost-sensitive systems. To overcome this limitation, sensorless control strategies have gained attention. This paper presents a comparative study of two sensorless control strategies for high-speed PMSMs: Field-Oriented Control (FOC) and Pulse Amplitude Modulation (PAM). The focus is on evaluating electromagnetic torque and current harmonics under a limited switching frequency of 10 kHz. In this study, sensorless FOC uses an open-loop flux observer to estimate rotor position, while PAM relies on detecting back-EMF zero crossings. Simulation results show that FOC provides smoother torque output compared to PAM, while both strategies ensure stable operation at 60,000 rpm. Moreover, PAM control has been experimentally validated on a prototype test bench.

Mots-clés—PMSMs, high-speed compressors, Field-Oriented Control, PAM, sensorless control, electromagnetic torque, switching frequency.

1. INTRODUCTION

Over the last few decades, the trend toward adopting high-speed PMSMs in various applications such as turbochargers, compressors, pumps, and blowers is justified by their remarkable benefits. These include high power density, reduced volume for the same power output, and good efficiency [1], [2]. The design of the electrical drive for high-speed PMSMs depends on the selection of the converter topology, control strategy, and whether or not including a rotor position sensor. This selection heavily depends on the intended application, which, in the context of this paper, involves driving an air conditioning compressor in an electric vehicle.

Researchers in [1], [2] and [3] have conducted an in-depth analysis of various converter topologies suitable for driving high-speed PMSM applications. This analysis includes PWM Voltage Source Inverters (VSI), DC-DC converter connected to a VSI, or a Current Source Inverters (CSI) among others. In our study, we are interested to a VSI. According to the parameters specified in Table I, the machine under consideration has small size and requires a stator voltage of approximately 40 Vrms at 60 krpm nominal speed (under no load condition). Due to the insufficient DC bus voltage of 48 V, it is necessary to integrate a DC-DC converter to step up the voltage at nominal speed.

Regarding the control strategies, the PMSM with sinusoidal back EMF can be driven with either square-wave current (BLDC operation) or sinusoidal current (BLAC operation) [4]. To determine the optimal control strategy that ensures both cost-effectiveness and good efficiency, a comprehensive performance analysis is essential. To achieve low-cost solutions, authors have focused on the analysis and comparison of BLDC drives: six step PWM control versus PAM method [2], [5], [6]. Authors in [7] and [8] compared FOC with six-step PWM control. A comparison between FOC and PAM method is crucial to determine if FOC can significantly reduce current harmonics compared to PAM control under limited switching frequency, thereby minimizing losses in the machine. A significant research gap exists in the direct comparison of FOC and PAM control for high-speed applications.

This paper aims to present and compare PAM control versus FOC for high-speed PMSMs, focusing on torque output and current harmonics. Both control methods will be implemented using low-cost solutions including the simplest form of sensorless control for each technique and operating at the minimum possible switching frequency.

Tableau 1. Parameters of PMSM drive system.

Parameters	**Value**
Stator resistance (R)	0.33 Ω
Stator inductance (L)	82 μH
Pole pairs (p)	1
Magnet flux linkage (ϕ_{PM})	6.18 mWb
Length	122.5 mm
Diameter	70 mm

2. ANALYTICAL EXPRESSION OF CURRENT AND ELECTROMAGNETIC TORQUE

Figure. 1 illustrate the ideal BLAC and BLDC operations of the PMSM. 'Ideal' here refers to operations without considering the freewheeling diode periods.

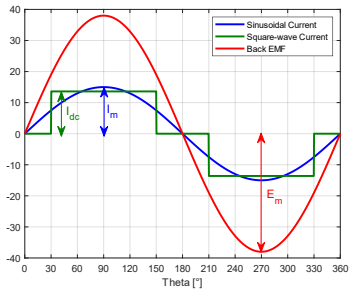

Fig. 1. Back EMF and ideal current waveforms as a function of rotor position.

For non-salient PMSM, the electromagnetic torque is expressed as :

$$T_{em} = \frac{1}{\Omega}(e_a i_a + e_b i_b + e_c i_c) \quad (1)$$

Where i_a, i_b and i_c are phase currents, Ω is mechanical speed and e_a, e_b and e_c are back EMF voltages.

In the stationary frame (Concordia transformation), the back EMF is written as :

$$\begin{bmatrix} e_\alpha \\ e_\beta \end{bmatrix} = \sqrt{\frac{2}{3}} \begin{bmatrix} 1 & -\frac{1}{2} & -\frac{1}{2} \\ 0 & \frac{\sqrt{3}}{2} & -\frac{\sqrt{3}}{2} \end{bmatrix} \begin{bmatrix} e_a \\ e_b \\ e_c \end{bmatrix}, \; e_a = -E_m \sin\theta_r \quad (2)$$

Where E_m is the amplitude of the back emf and θ_r is the rotor position. The complex vector representation of the three-phase back EMF is [9]:

$$\overline{e_{\alpha\beta}} = e_\alpha + j e_\beta = \left|\overline{e_{\alpha\beta}}\right| e^{j\theta_e} = \sqrt{\frac{3}{2}} E_m e^{j\left(\theta_r + \frac{\pi}{2}\right)} \quad (3)$$

2.1. *FOC control*

In FOC control, the complex current vector is a continuously rotating vector (considering MTPA control) :

$$\overline{i_{\alpha\beta}} = \left|\overline{i_{\alpha\beta}}\right| e^{j\theta_{FOC}} = \sqrt{\frac{3}{2}} I_m e^{j\left(\theta_r + \frac{\pi}{2}\right)} \quad (4)$$

Consequently, the electromagnetic torque can be written as :

$$T_{em} = \frac{\overline{e_{\alpha\beta}} . \overline{i_{\alpha\beta}}}{\Omega} = \frac{3}{2}\frac{E_m I_m}{\Omega} \quad (5)$$

2.2. *PAM control*

Under PAM control, the inverter operates in six step (120° conduction) mode, and the motor speed is regulated by varying the DC-link voltage at the inverter input [8]. Six step operation consists of energizing two phases simultaneously at each 60° interval of the electrical cycle, while the third phase is left floating [4]. The current vector is a discretely rotating vector. The calculation of current complex vector will be performed in sector 2, when $30° \leq \theta_r \leq 90°$, and the same analysis applies to the other sectors. The three phase current are :

$$\begin{cases} i_a = -I_{dc} \\ i_b = I_{dc} \\ i_c = 0 \end{cases} \quad (6)$$

It is noted that the convention here that the back EMF are as shown in Fig. 2.

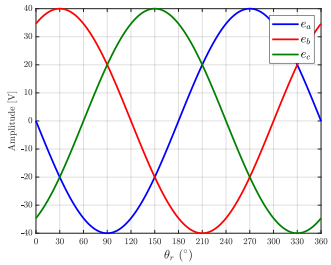

Fig. 2. Sinusoidal back EMF waveforms assumptions.

In the stationary frame,

$$\begin{bmatrix} i_\alpha \\ i_\beta \end{bmatrix} = \sqrt{\frac{2}{3}} \begin{bmatrix} 1 & -\frac{1}{2} & -\frac{1}{2} \\ 0 & \frac{\sqrt{3}}{2} & -\frac{\sqrt{3}}{2} \end{bmatrix} \begin{bmatrix} -I_{dc} \\ I_{dc} \\ 0 \end{bmatrix} \quad (7)$$

Therefore, the current complex notation is given by,

$$\overline{i_{\alpha\beta}} = \left|\overline{i_{\alpha\beta}}\right| e^{j\theta_{PAM}} = \sqrt{2} I_{dc} e^{j\left(\frac{5\pi}{6}\right)} \quad (8)$$

Consequently, T_{em} in sector 2 can be written as,

$$T_{em} = \frac{\overline{e_{\alpha\beta}} . \overline{i_{\alpha\beta}}}{\Omega} = \frac{\sqrt{3} E_m I_{dc} \cos(\theta_r + \frac{\pi}{2} - \frac{5\pi}{6})}{\Omega} \quad (9)$$

Figure. 3 shows the waveform of T_{em} during an electrical cycle.

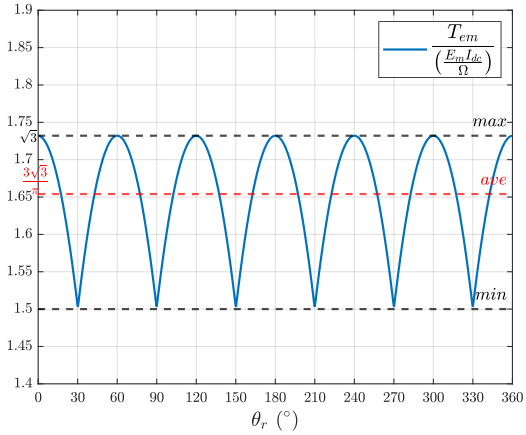

Fig. 3. The normalized electromagnetic torque waveform during a cycle under six step control.

2.3. *Analytical comparison*

Figures. 4a and 4b illustrate the ideal back EMF and current vectors for PAM (six step inverter operation) and FOC control, respectively, with MTPA adopted. In Fig. 4a, the angle between $\overline{e_{\alpha\beta}}$ and $\overline{i_{\alpha\beta}}$ vectors changes with the rotor position, being zero at the middle of each sector. In contrast, for the FOC, since the rotor position is continuously measured, the angle is always zero. The torque is imposed and is the same for both operations; therefore, using Eq. 5 and Eq. 9, the relation between currents is:

$$I_{dc} = 0.907 I_m \quad (10)$$

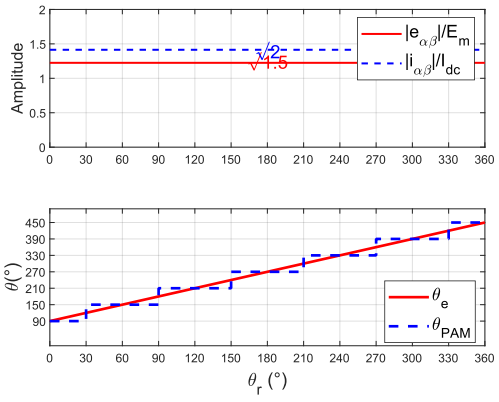

(a)

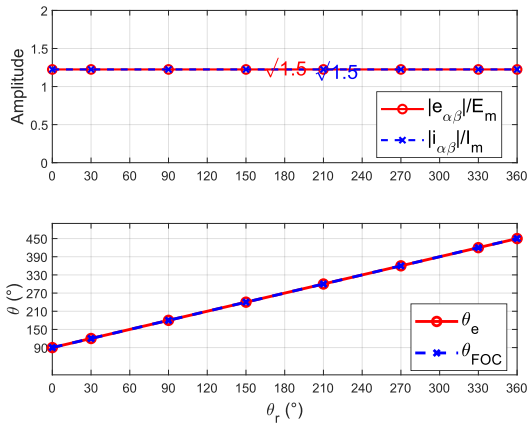

(b)

Fig. 4. The ideal waveforms of current and back EMF vector (a) six step control (b) FOC control.

3. PMSM DRIVE

3.1. *FOC drive*

Figure. 5 illustrates the converter topology. The DC-DC converter is a boost converter because to reach the operating speed of 60 krpm, 48V is not sufficient. In the literature, voltage reference on the input of the inverter is generated using the closed loop structure of the FOC control or it can be fixed. In this article, the model of the PMSM in Park coordinate is used to estimate the reference voltage at the input of the inverter. Figures. 6 and 7 show the current and voltage regulators, respectively, of the boost converter, which operates with a cascaded control scheme. Figure. 8 shows the overall block diagram of the FOC drive. A continuous rotor position is needed in FOC control. One of the simplest sensorless techniques, the open-loop flux observer in the alpha-beta frame, is commonly used to continuously estimate the rotor position without physical sensors [10].

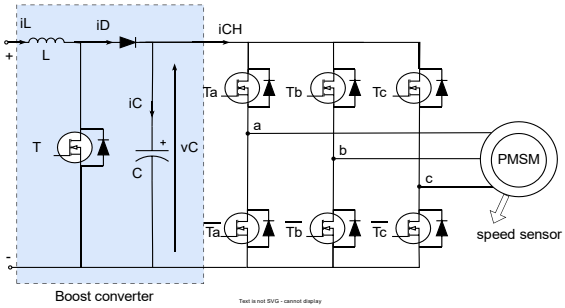

Fig. 5. Boost converter connected to the front-end of the VSI inverter.

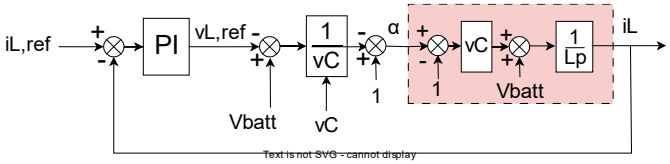

Fig. 6. Current regulator of the boost converter.

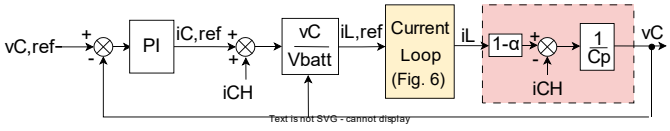

Fig. 7. Voltage regulator of the boost converter.

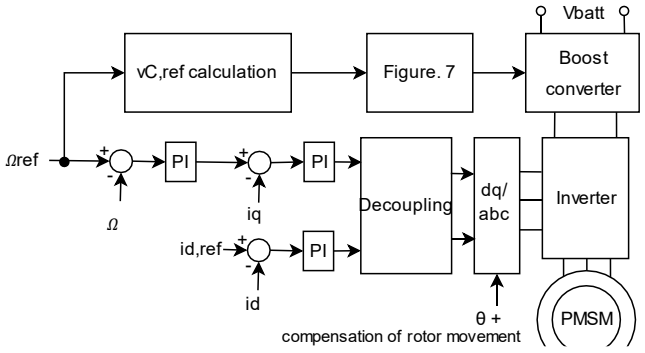

Fig. 8. Control block diagram of the PMSM.

3.2. *PAM Drive*

In such drive, the inverter is switched at the motor's fundamental frequency while the DC-DC converter adjust the voltage at the input of the VSI according to the desired speed. To operate under a wide speed range, the DC-DC converter is a buck-boost (see Fig. 9). The output voltage of the converter is regulated according to the reference speed as shown in Fig. 10. The simplest sensorless methods commonly used for six step control are based on detecting the zero crossing of the back EMF. The authors in [4] review these methods. Since two phases are conducting at any time, the zero crossing (ZC) of back EMF can be detected on the floating phases. In this paper, a method based on the terminal voltage using a LPF is implemented to achieve a satisfactory speed range. At higher speeds, the phase delay between the current and back EMF caused by the free-wheeling periods can become significant and requires further study. In this article, the compensation algorithm presented in [9] is used.

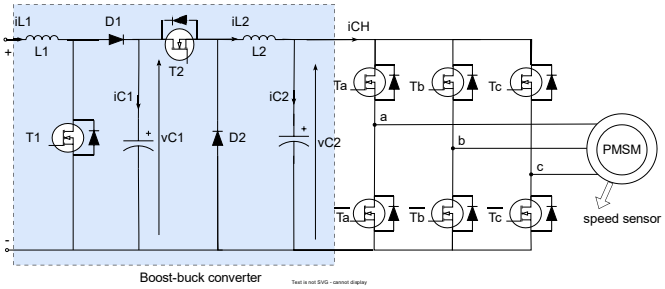

Fig. 9. Boost-buck converter connected to the front-end of the VSI inverter.

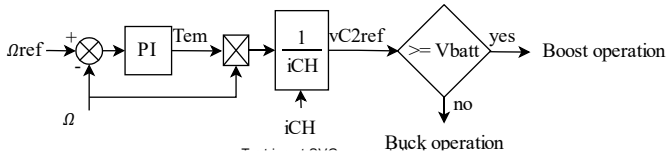

Fig. 10. Speed regulator of the boost-buck converter under PAM control.

4. SIMULATION RESULTS

The FOC and PAM drive control for the PMSM were simulated in MATLAB/Simulink, with the compressor operating at 60 krpm. Fig. 11 and 12 show the phase current and electromagnetic torque under FOC. The Total Harmonic Distortion (THD) in the torque is measured at 7%, and the phase current THD is 10%. Fig. 13 presents the system's behavior during the transition to sensorless FOC control, alongside a speed reference adjustment from 60 to 30 krpm. The sensorless control is capable of operating from a speed of approximately 5,000 rpm. Despite the overall stability during the transition, the torque and current exhibit a noticeable

decline in performance during transient, largely due to the delay impacting higher speed operations.

Figures. 14 and 15 show the phase current and electromagnetic torque under PAM control. The THD is significantly higher compared to FOC, with the torque THD reaching 15.3% and the phase current THD measured at 30%, as shown in Figs. 16 and 17. The dominant harmonic in the electromagnetic torque is the 6th harmonic, which contributes to ripple in the torque waveform, leading to increased mechanical vibrations. Meanwhile, the phase current is primarily dominated by the 5th and 7th harmonics, which can result in higher power losses and reduced efficiency. The sensorless algorithm for the PAM drive is also evaluated. In steady state at t = 0.2 s, the control of the switches is achieved through the implemented sensorless algorithm. The RMS value of the current increases slightly, as shown in Fig. 18. However, this increase is not significant and is due to the phase delay introduced by the LPF. Fig. 19 shows the dynamic performance during the transition to sensorless control and the speed reference change from 60 to 40 krpm. The sensorless control is able to operate starting from a lower speed of about 20 krpm. The system remains stable throughout the transition, demonstrating the robustness of the control strategy. To assess the impact of the phase delay error between the current and back EMF caused by the freewheeling periods on the performance of the PAM drive, the worst-case scenario was analyzed at a speed of 60 krpm. Even though the phase delay was 4° and was compensated for, the reduction in current is not significant, as shown in Fig. 20. This reduction is not important since the torque is still considered light.

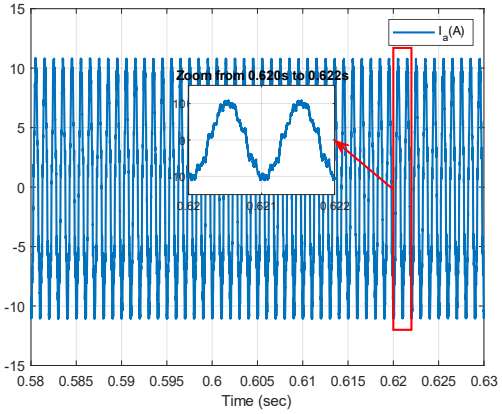

Fig. 11. Current waveform under FOC control.

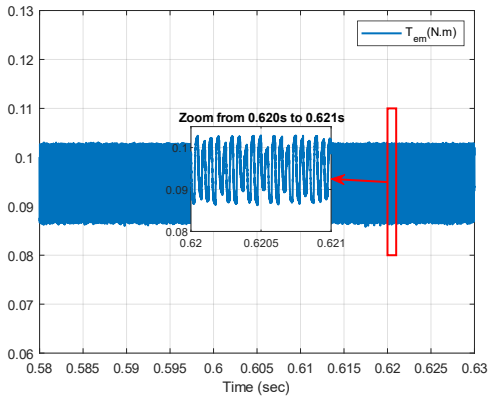

Fig. 12. Electromagnetic torque waveform under FOC control.

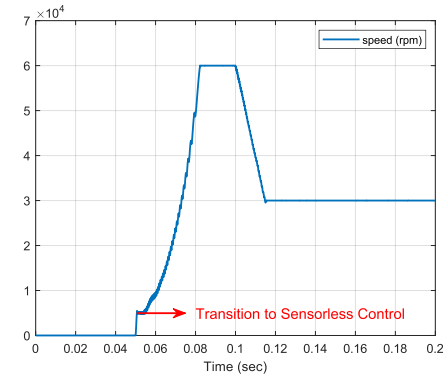

Fig. 13. Dynamic performance during the transition to FOC sensorless control and speed reference change from 60 to 30 krpm. Sensor-based start.

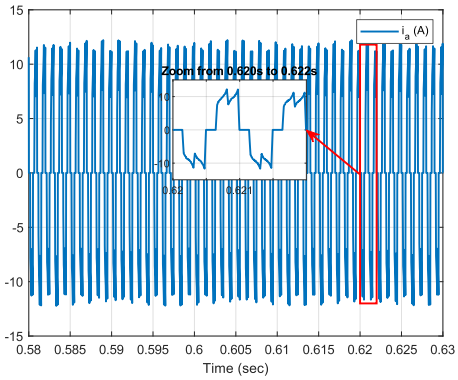

Fig. 14. Current waveform under PAM technique.

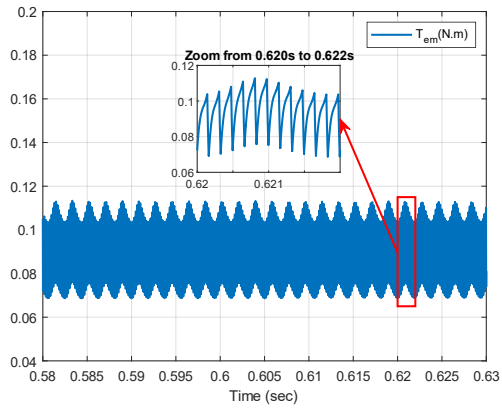

Fig. 15. Electromagnetic torque waveform under PAM control.

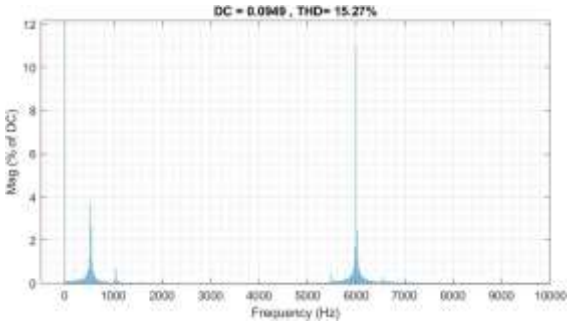

Fig. 16. FFT spectrum of the electromagnetic torque under PAM control.

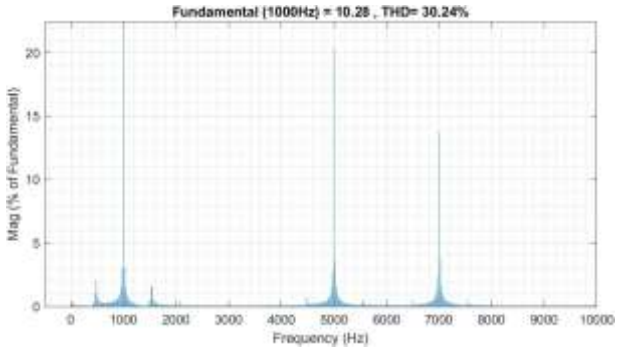

Fig. 17. FFT spectrum of the phase current under PAM control.

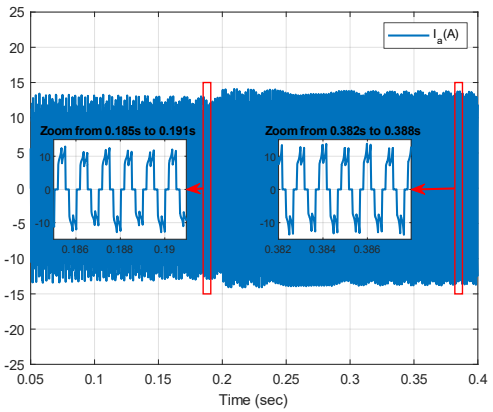

Fig. 18. Phase current under 60 krpm. At t=0.2, the control is switched to the sensorless algorithm.

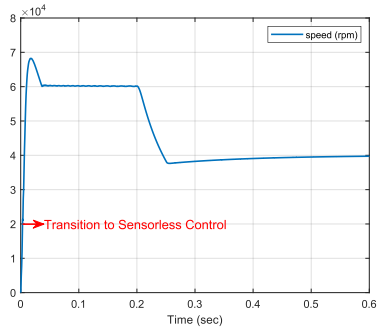

Fig. 19. Dynamic performance during the transition to PAM sensorless control and speed reference change from 60 to 40 krpm. Sensor-based start.

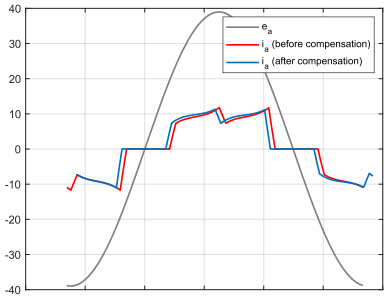

Fig. 20. The current and back EMF waveforms at a speed of 60 krpm and a load torque of 0.095 N.m.

5. Experimental Results

This section presents the experimental validation of the PAM control strategy for the high-speed PMSM drive system. Figure. 21a shows the boost-buck converter and the two level VSI supplied by a 20V DC source with a current limit of 20A. The PMSM setup is shown in Fig. 21b, and its parameters are listed in Table 1. Real time control of both the DC-DC converter and the inverter is implemented in dSPACE platform. The PWM frequency of the DC-DC converter is set at 10 kHz and the dSPACE sampling frequency is set to 50 kHz. A conventional three-stage starting strategy is implemented to start the PMSM.

Figure 22 presents the experimental waveforms (Test 1) obtained under no-load conditions, where the motor speed increases from 3,000 to 35 krpm before decreasing back to 3,000 rpm (see Fig. 23). The phase currents i_a and i_b are shown in Fig. 22 (top plot), while the middle plot illustrates the voltage at the input of the buck converter (vC1) and the voltage at the input of the VSI (vC2). The bottom plot displays the terminal voltages (Vao, Vbo and Vco), defined with respect to the midpoint of the DC bus. Zoomed-in views in the top and bottom plots highlight the waveforms of i_a and Vao at 35krpm. Figure 24 shows the experimental waveforms (Test 2), also under no-load conditions, in which the speed increases from 3,000 to 52,000 rpm and then decreases to 3,000 rpm (see Fig. 25). Figure 26 presents the control signal of the buck-boost converter along with the inductor currents iL1 and iL2 under Test 2.

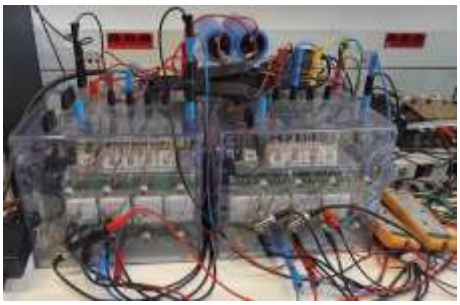

(a)

(b)

Fig. 21. Experimental platform (a) power electronic converter (b) PMSM.

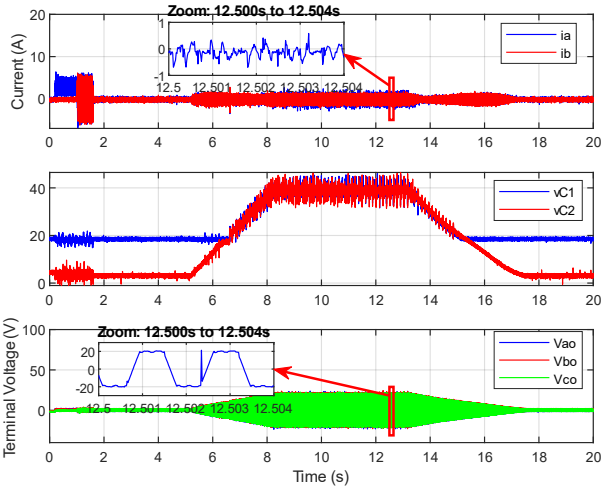

Fig. 22. Experimental waveforms under no-load condition (Test 1) with speed transition from 3,000 to 35,500 rpm and back.

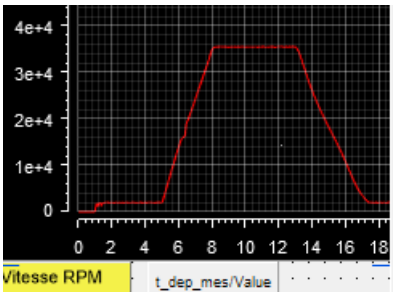

Fig. 23. Speed measurement (test 1).

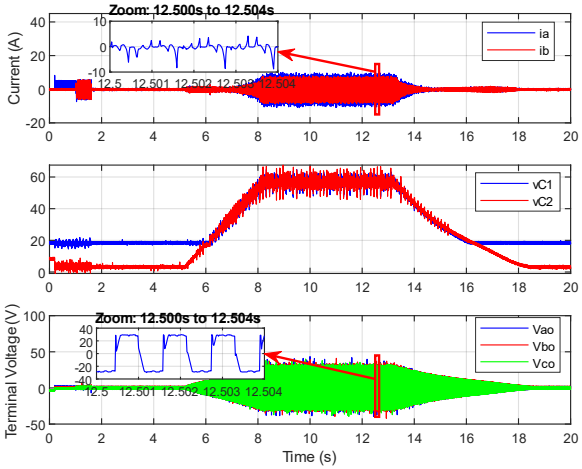

Fig. 24. Experimental waveforms under no-load condition (Test 2) with speed transition from 3,000 to 52,000 rpm and back..

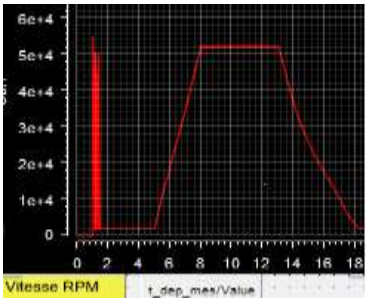

Fig. 25. Speed measurement (test 2).

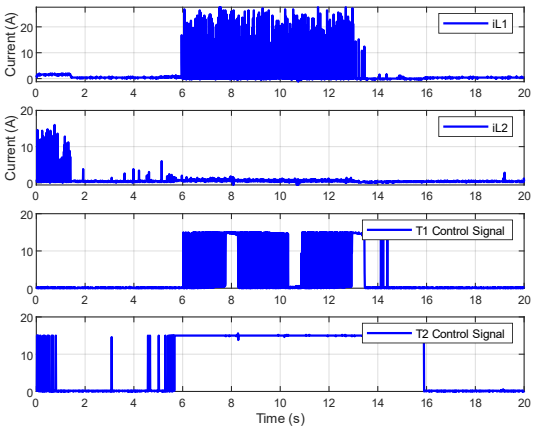

Fig. 26. Experimental waveforms of the buck-boost converter under no-load condition (Test 2): inductor currents iL1, iL2, and control signals of switches T1 and T2.

6. Conclusions

In this article, a comparison of two electrical drives is conducted under a limited switching frequency of 10 kHz. The low harmonic content in FOC electromagnetic torque results in smoother torque production and reduced mechanical vibrations. The current harmonic reduction contributes to more efficient operation, minimizing power losses and enhancing overall performance. However, this comes at the cost of higher expense and computational power. Among the simplest sensorless algorithms, FOC still requires the calculation of Clarke transformations and precise rotor position estimation. An experimental platform was developed to validate the effectiveness of PAM control using a simple ZC method to operate a high-speed PMSM at 52krpm. The analysis presented in this article offers valuable insights into both PAM control and FOC, which can help in selecting the appropriate control strategy and addressing specific challenges, particularly in high-speed applications. As future work, experimental validation of FOC and a finite element method (FEM) analysis are suggested. Specifically, the harmonic content should be quantified using FEM to assess whether machine losses under PAM control become significant compared to FOC.

7. References

[1] L. Wang, Z.-Q. Zhu, H. Bin, and L. Gong, “Recent developments of high speed electrical machine drive systems,” in 2021 Sixteenth International Conference on Ecological Vehicles and Renewable Energies (EVER), 2021, pp. 1–10.

[2] C. Zwyssig, S. D. Round, and J. W. Kolar, “An ultrahigh-speed, low power electrical drive system,” IEEE Transactions on Industrial Electronics, vol. 55, no. 2, pp. 577–585, 2008.

[3] C. Zwyssig, S. Round, and J. W. Kolar, “Power electronics interface for a 100 W, 500000 rpm gas turbine portable power unit,” in Twenty-First Annual IEEE Applied Power Electronics Conference and Exposition, 2006. APEC’06., 2006, pp. 7-pp.

[4] C B. Zbib, F. Chabour, H. Taha, and G. Barakat, “Sensorless Trapezoidal Control of Brushless Permanent Magnet Motors: Review on Back EMF Position Sensing Techniques,” in International Conference of the TC Electrimacs Committee, 2024, pp. 645–658.

[5] M. R. Rusli, H. Rahmatullah, M. B. Fauziah, A. Jaya, M. M. Rifadil, and E. Purwanto, “Pulse width modulation (PWM) and pulse amplitude modulation (PAM) technique for medium-speed BLDCM in electric vehicle application,” in 2018 International Seminar on Application for Technology of Information and Communication, 2018, pp. 87–92.

[6] Y.-S. Lai, K.-Y. Lee, J.-H. Tseng, Y.-C. Chen, and T.-L. Hsiao, “Efficiency comparison of PWM-controlled and PAM-controlled sensorless BLDCM drives for refrigerator applications,” in 2007 IEEE Industry Applications Annual Meeting, 2007, pp. 268–273.

[7] C.-L. Huang, G.-R. Chen, S.-C. Yang, and Y.-L. Hsu, “Comparison of high speed permanent magnet machine sensorless drive using trapezoidal BLDC and sinusoidal FOC under insufficient PWM frequency,” in 2019 IEEE Energy Conversion Congress and Exposition (ECCE), 2019, pp. 321–325.

[8] F. Li, W. Yao, and K. Lee, “Quantitative characteristic comparison between sensorless six step and field oriented control methods for permanent magnet brushless DC motors,” in 2019 IEEE Energy Conversion Congress and Exposition (ECCE), 2019, pp. 1881–1885.

[9] B. Tan, X. Wang, D. Zhao, K. Shen, J. Zhao, and X. Ding, “A lag angle compensation strategy of phase current for high-speed BLDC motors,” IEEE Access, vol. 7, pp. 9566–9574, 2018.

[10] T.-D. Ton, M.-F. Hsieh, and P.-H. Chen, “A novel robust sensorless technique for field-oriented control drive of permanent magnet synchronous motor,” IEEE Access, vol. 9, pp. 100882–100894, 2021.